Development of the GridPix detector quad

Talk presented at the 9th Symposium on Large TPCs for Low-Energy Rare Event Detection at Diderot University (Paris, France) on 12 – 14 December 2018

Yevgen Bilevych[1], Klaus Desch[1], Jean-Paul Fransen[2], Harry van der Graaf[2], Markus Gruber[1], Fred Hartjes[2], Bas van der Heijden[2], Kevin Heijhoff[2], Charles Ietswaard[2], Dimitri John[2], Jochen Kaminski[1], Peter Kluit[2], Naomi van der Kolk[2], Auke Korporaal[2], Cornelis Ligtenberg[2], Oscar van Petten[2], Gerhard Raven[2], Joop Rövekamp[2], Lucian Scharenberg[1], Tobias Schiffer[1], Sebastian Schmidt[1] and Jan Timmermans[2]

[1]Physikalisch Institut, University of Bonn, Nuβallee 12, 53115 Bonn, Germany
[2]Nikhef, PB41882, 1009DB Amsterdam, Netherlands

Corresponding author: Fred Hartjes f.hartjes@nikhef.nl

Abstract. We have developed the gaseous GridPix detector *quad* made from four Timepix3 chips. To provide the required charge amplification a Micromegas-like grid has been deposited on the chip surface by MEMS technology. The grid holes are precisely aligned to the chip pixels and have a pitch of 55 µm while the high time resolution of 1.56 ns of the Timepix3 chip enables the precise reconstruction of each individual primary ionization electron in the detector gas. The chip is coated by a high resistivity protection layer to prevent damage by unavoidable discharges. Using the GridPix technology, the full position of the ionization cloud is measured. As such the ultimate resolution of a gaseous detector is achieved, mainly limited by diffusion. The quad has all services located under the detection surface. Multiple quads can be simply joined together to create a large readout plane of a TPC. In this paper we show details about the construction of the quad and the preliminary results from a recent test beam experiment at the ELSA electron beam facility in Bonn.

1. Introduction

The GridPix technology, using the pixel chip Timepix or Medipix equipped with a Micromegas grid by MEMS technology, has been described in a series of papers [1]. The combination of a moderate gas amplification (2000 – 5000) with a low discriminator threshold (500 - 1000 e^-) enables the detection of single electrons. The Timepix has a fine pixel pitch of 55 x 55 μm^2 and 256 x 256 pixels. Since the diffusion of electrons in the ionization cloud drifting in the gas mostly exceeds 100 µm, a GridPix detector using the Timepix merely registers single electrons, only blurred by diffusion.

For each hit on a pixel of the Timepix, the time of arrival relative to an external trigger signal is registered with ≥10 ns time bins. However, because of the finite rise time of the signal at the discriminator input and the additional delay for small signals, additional time delay occurs, sometimes exceeding 100 ns. This so-called time slewing effect worsens the resolution in the drift direction.

In 2015 a number of Timepix3 chips [2], the successor of the first generation Timepix chip, were successfully equipped with a Micromegas grid. In this chip, the registration of the time of arrival has been greatly improved by the refined time resolution of 1.56 ns. Since the duration of the charge signal is registered as the Time over Threshold (ToT), the time walk error can be for a great deal corrected, resulting in an improvement of the position resolution in the drift direction.

A gaseous detector made with a single Timepix3 chip has been tested in 2017 in a 2.5 GeV electron beam at ELSA (Bonn). The detector was filled with an $Ar/CF_4/iC_4H_{10}$ 95/3/2 mixture. A grid voltage up to 350 V and a drift field of 280 V/cm were applied. As a reference for the tracks we used a Mimosa26 silicon telescope [3] placed upstream of the detector. The results [4] for the transverse diffusion coefficient are $306\ \mu m/\sqrt{cm}$ and for the longitudinal diffusion coefficient $226\ \mu m/\sqrt{cm}$. Both values approach closely the expected diffusion for this gas mixture.

From the data we investigated the systematic deviations across the pixel plane (x, y). The pixel plane was divided in 64 x 64 squares of 4 x 4 pixels to reduce the statistical error of the limited number of hits per pixel. A spread on deviations over the detector plane of 7 µm in x direction was observed. In drift direction (z) the spread was found to be 21 µm.

Another advantage of individually detecting all electrons is a precise energy loss dE/dx measurement by counting electrons. Here the ultimate resolution is achieved by sampling across a gas volume. The data show a standard deviation for the 2.5 GeV electrons of 4.1% for a meter track length. The separation between an electron and a MIP was measured to be 6.2 σ [4].

The successful operation of the GridPix detector based on Timepix3 inspired us to use Timepix3 based detectors to cover a large TPC detection area. To maximize the sensitive area of the chip, the control and output lines were directed to the backside of the chips. Also the LV supply regulation and grid voltage filtering board were put in this space. When building large detection areas, it is practical to subdivide the detection surface into a number of standardized modules. Because of the complexity of the GridPix technology and the fragility of the grids, it is wise to start with a small number of chips per standard module. Therefore, we have chosen to confine the standard GridPix module to an assembly of four Timepix3 chips, the *quad*, as a first step.

2. Construction of the quad

2.1. *Timepix3 as a GridPix detector*

To convert a Timepix3 chip into a GridPix detector, at first a continuous 4 µm thick resistive Si_xN_y protection layer was deposited across the whole surface, leaving only the wirebond pads uncovered. The volume resistivity of the layer is of the order of 10^{11} Ωm to avoid permanent charge build up by the avalanches. Subsequently, a 1 µm thick aluminium grid is deposited on the chip, supported by 50 µm high insulating pillars from SU8. The grid contains a matrix pattern of 35 µm wide holes aligned to the pixel pads. At the two side edges, the grid ends in a 150 µm wide dyke from solid SU8 to get a proper mechanical termination of the fragile grid and to avoid high electrical fields at the grid edges. For the dykes 3 columns of 256 pixels had to be covered on each side. At the wirebond side and the side opposite to it, the dyke is 1000 and 400 µm wide respectively. No pixels had to be sacrificed for this. Figure 1 shows the surface of the Timepix3 chip equipped with the grid and wirebonds. The area for the chip electronics, wirebond pads and the wirebond board is indicated by the 5 mm wide red dashed rectangle.

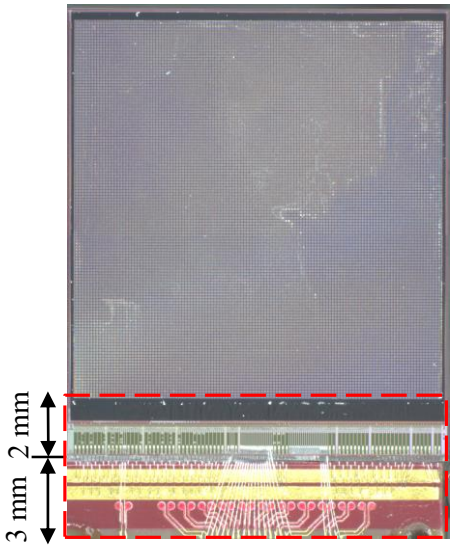

Figure 1. Timepix3 chip (top view) and its connection to the wirebond board.

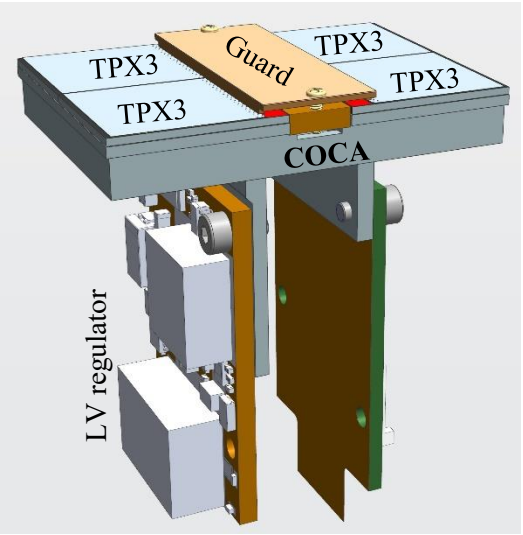

Figure 2. Assembly of the quad with four Timepix3 chips mounted on the COld CArrier (COCA). The central guard electrode and LV regulator are also shown.

2.2. Assembly of the quad

Mechanically, the quad consists of a baseplate carrying the four Timepix3 chips and providing the cooling, called COCA. The chips are electrically connected by wirebonds to a 6 mm wide PCB between the two pairs of chips (figure 2). This width is the minimum that can be achieved by today's technology to house the very dense structure of signal traces for control and output. The wirebond PCB ends at one edge into a 15 cm long Kapton cable containing the control lines and output lines of the chips (second picture figure 3) and is bended downwards under the COCA. A short Kapton cable at the other edge of the wirebond PCB provides a low impedance connection to the low voltage (LV) regulator. Note that the whole assembly of wirebond board, output flex and LV regulator is manufactured as a single item. As such it forms the heart of the quad.

The grids are connected by a 63.5 µm insulated magnet wire (Temco Industrial) to an HV filtering board. The connection to the common HV input passes a 100 MΩ resistor for each grid to rapidly quench a micro-discharge. To minimize the electrical energy on the grids, no filtering capacitors are added, only the grid has its parasitic capacity of 35 pF. To support and cool the LV regulator board and the HV filtering board, a U-shaped support is attached by thermally conductive glue under the COCA. Finally, the wirebonds of the quad are covered by a 10 mm wide central guard electrode located 1.1 mm above the grids to maintain a linear drift field. In the present design, the COCA and the U-shaped support are made of aluminium.

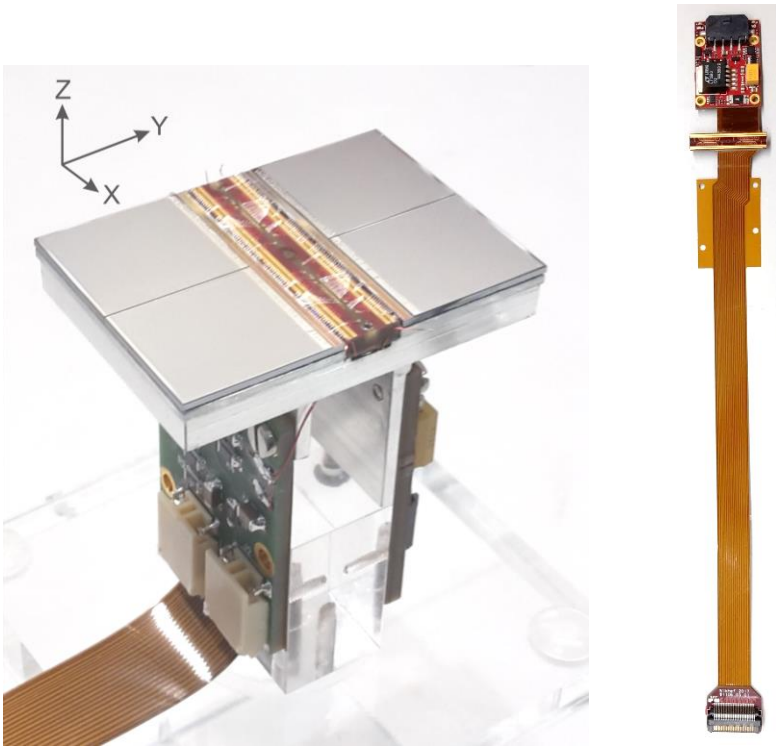

Figure 3. An assembled quad detector (left) and the wirebond board (right) with the flexible Kapton cables and low voltage stabilizer. The central guard electrode has been omitted to show the wirebond PCB.

The quad is designed to achieve the highest coverage of the detection area that can be obtained with Timepix3 chips equipped with an InGrid and using wirebond connections. The matrix of active pixels is 250 x 256 large, 2 x 3 columns are covered by the side dykes. The edge of the COCA only extends by 12 µm nominally outside the edge of the four Timepix3 chips that are approximately 16.65 x 14.15 mm large. Together with the 6 mm wide wirebond PCB we thus get an external quad dimension of 39.6 x 28.38 mm of which 68.9% is active. Since all services are located under the COCA surface, on each edge other quads can be joined to create large TPC detection surfaces.

3. Measuring the performance of the quad in the ELSA testbeam

3.1. Making a TPC from the quad

To make a TPC we added a 40 mm high field cage to the quad to create a homogeneous drift field. The sides of the field cage were formed by 75 µm CuBe field shaping wires with a 2 mm pitch (figure 4). We applied this solution instead of more solid field shaping electrodes to facilitate measurements with an ionizing UV laser beam. A solid drift cathode plate terminated the field cage. The opposite side of the drift cathode was made of a coppered frame, closely surrounding the quad and mounted at the same level as the quad. The whole structure was put in a gastight container.

The potentials of all electrodes and the grids were regulated by four HV power supplies under LabVIEW control. The program used as an input the grid voltage and the value of the drift field to calculate and set all potentials.

3.2. *Setup at the testbeam*

To investigate the quad's ability to measure high momenta charged particle tracks, we have installed a quad detector in the ELSA testbeam at Bonn University in October 2018. The quad TPC was sandwiched between 2 x 3 planes of the Mimosa26 telescope. Each telescope plane used a MAPS pixel detector with 18.4 µm pitch and an acceptance of 21.2 x 10.6 mm in the xz plane (figure 4).

The readout of the quad was done with a SPIDR board and the related software [5]. It works in the data driven mode i.e. each hit on a pixel is stored as the pixel's address and a 4 + 14 bit time stamp with a resolution of 1.56 ns. The separate trigger input of the SPIDR board was connected to the discriminated scintillator signal. The trigger time stamps were added to the SPIDR data stream.

The telescope hits were collected in time frames of 115.2 µs without further time information. But the telescope and trigger timestamps are linked by the trigger number. Due to the high beam intensity, often the telescope frame contained the data of more than one track.

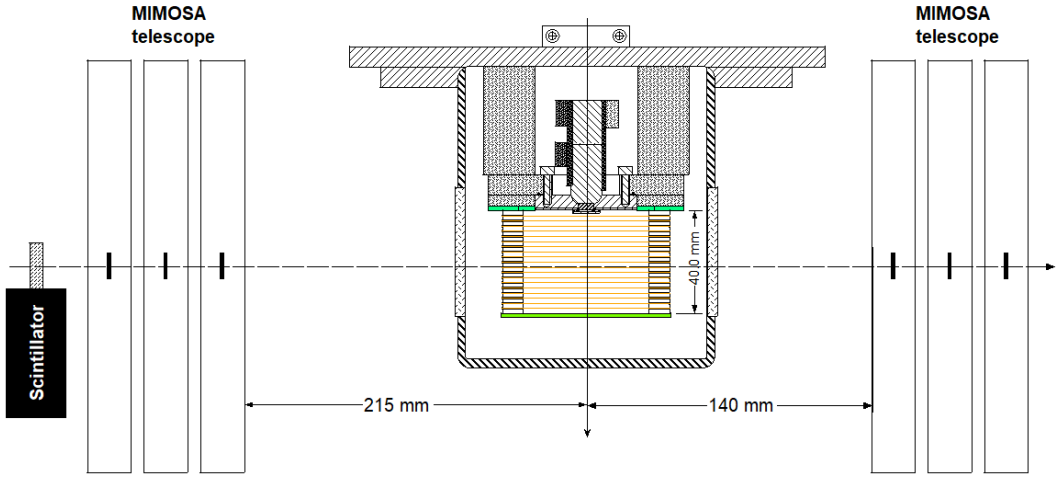

Figure 4. Setup of the quad in the ELSA testbeam

3.3. Experimental conditions

The chamber was flushed with an $Ar/CF_4/iC_4H_{10}$ 95/3/2 mixture. The drift field was set at 280 V/cm, the point where the drift velocity is expected to be at its maximum. The grid voltage was set at 300 V. Also runs at higher grid voltages and higher single electron efficiencies were taken. The threshold was set at about 550 e^-. The beam rate was approximately 10 kHz. In addition, many background tracks were present, so tight cuts had to be taken to select only proper tracks. The beam was passing the drift volume almost parallel to the y axis of the quad (figure 3) and also parallel to its xy plane.

During data taking a log file was created where every minute the electrode potentials, gas flow, oxygen concentration, temperature of the quad cooling plate and absolute pressure were recorded.
For the testbeam we initially used a quad from the first production series having a poorer quality of the grids. The analysis in this paper uses exclusively data from this quad. Data from a second quad with better grids are presently under investigation.

4. Analysis

At the time of the conference, the data analysis was still in progress, so only preliminary results are given in this report. Here the data of run 627 will be discussed. The combination of telescope acceptance and beam width in z (18 and 10 mm respectively), enabled us to measure the drift velocity and diffusion as a function of z. In total approximately 8000 tracks were selected that passed the criteria of table 1.

Table 1. Selection criteria for accepted tracks

Criterion	Explanation
$-500\ \text{ns} < t_{hit} - t_{trigger} < 500\ \text{ns}$	Reject out of range drift times
$\text{ToT} > 0.10\ \mu\text{s}$	Reject small signals (large time walk)
$res_x < 1.5\ \text{mm};\ res_z < 3\ \text{mm}$	Reject outliers
$N_{hits} > 20$	Reject poorly defined tracks
$(N_{res_x} < 1.5\ \text{mm})/(N_{res_x} < 5\ \text{mm}) > 0.8$	Reject scattered tracks
$\lvert\overline{x_{hit}} - \overline{x_{track}}\rvert < 0.3\ \text{mm}$	Reject bad fits

where res_x and res_z are the residuals with respect to the track in the x (transverse) and z (drift) plane.

4.1. *Time walk correction*

There is a correlation between the residuals and the magnitude of the charge signal, measured as the ToT value. The measured correlation curve can be approximated by a simple expression:

$$\delta_{z_{timewalk}} = \frac{c_1}{t_{ToT}+t_0} \qquad (1)$$

where $\delta_{z_{timewalk}}$ is the error in z caused by the time walk, t_{ToT} is the duration of the charge signal and t_0 is a constant. The red curve of expression (1) shows a quite good agreement with the experimental data in figure 5. The residuals in z of the corrected hit values shown in figure 6, show a considerably improved accuracy and a curve that approaches a Gaussian distribution.

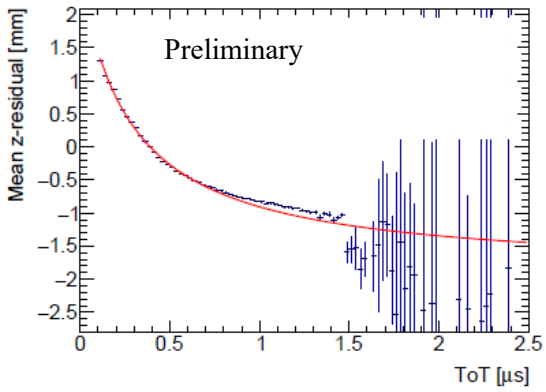

Figure 5. Averaged relation between z residuals and ToT.

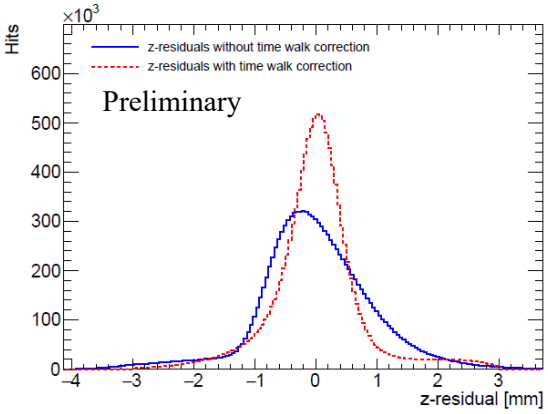

Figure 6. z residuals before and after ToT correction.

We applied the time walk correction for all following results in this paper.

4.2. Diffusion

From the distance between the individual hits and the projection of the fitted track on the Timepix3 surface the residuals in x were calculated as a function of the drift distance (figure 7). The diffusion function (2) was fitted through the data points:

$$\sigma_x = \sqrt{\sigma_0^2 + D_T^2(z - z_0)} \qquad (2)$$

where σ_x is the measured residual, σ_0 and z_0 (≈ 3.5 mm) are constants and D_T is the transverse diffusion parameter. The fit gave as a preliminary result a value of $D_T = 361\ \mu\text{m}/\sqrt{\text{cm}}$.

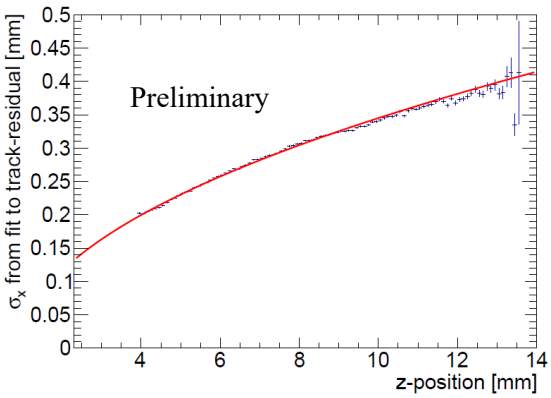

Figure 7. Transverse diffusion as a function of the predicted z position.

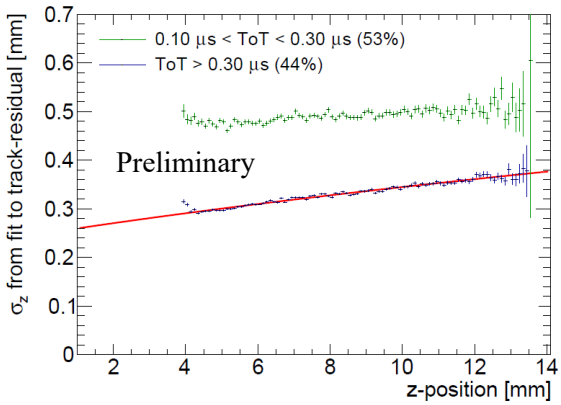

Figure 8. Longitudinal diffusion as a function of the predicted z position.

In the longitudinal direction the resolution σ_z is described by

$$\sigma_z = \sqrt{\frac{\tau^2 v_{drift}^2}{12} + \sigma_{z_0}^2 + D_L^2 (z - z_0)} \qquad (3)$$

where τ is the size of the time bin and v_{drift} is the drift velocity. σ_{z_0} is a constant determined by electronic noise, D_L and z_0 are a constant. The drift velocity v_{drift} was calibrated using the telescope and measured to be 56.7µm/ns. For this measurement the first term in expression (3) is about 25.5 µm, σ_{z_0} about 200 µm and z_0 is 3.5 mm. In the blue data points small charge signals with ToT < 0.3 µs are excluded. The slope of the curve in figure 8 corresponds to $D_L = 240\ \mu\text{m}/\sqrt{\text{cm}}$. The green data points for small signals have a higher value for σ_{z_0} but the curve shows a similar tendency.

4.3. *Field deformation in the inter-chip region*

At the present construction of the quad, a small distortion of the drift field at the boundary between two Timepix3 chips is expected (figure 9). While above the grid a constant potential is maintained, at the edge of the chip this is different. The dyke, partly covered by aluminium, partly insulated, ends just before the edge of the Timepix3 die. The grounded region between both chips is 50 – 100 µm wide.

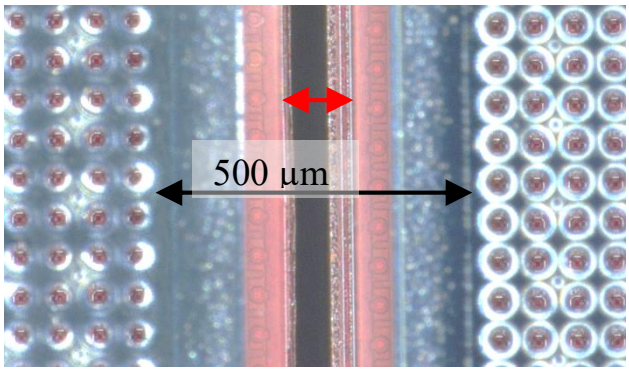

Figure 9. The boundary between two Timepix3 chips. The two pink bands are the uncovered zones of the dykes. The red arrow indicates the grounded region.

The resulting deformations in the drift field lead to deviations in the resolution in the xy plane, the electrons following the field lines are bent towards the grounded region. Many electrons will be suck into the ground well and thus remain undetected. But others further away from the well will follow a bended field line and end up at the wrong pixel.

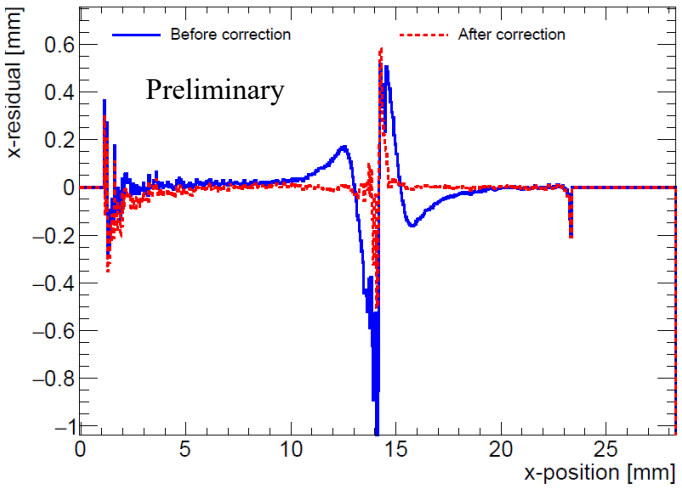

Figure 10. Averaged residuals in x across the detection surface. In red the residuals after correction are shown.

In figure 10 in blue the residuals in xy in the x direction are shown. At several mm from the inter-chip boundary there is a systematic shift towards the boundary rising to 180 µm at 1 mm distance. But at much closer distance part of the ionization electrons remain undetected, resulting in a systematic shift of the detected electrons in the opposite direction.

These two effects can be quite well compensated by adding an analytical correction as shown in red in figure 10.

4.4. Residuals in the xy plane

Figure 11 shows the average residual in the xy plane after the correction on the inter-chip boundary that is given in section 4.4. To get a clear picture with sufficient statistics per bin, the deviations were averaged over 4 pixels. In most areas the deviations from zero are smaller than 20 µm.

Due to the acceptance of the telescope and the width of the beam, the measurements of run 627 did not cover the whole active area of the quad. In addition, a few white spots are visible from damages on the grids. The new series quad does not have these defects.

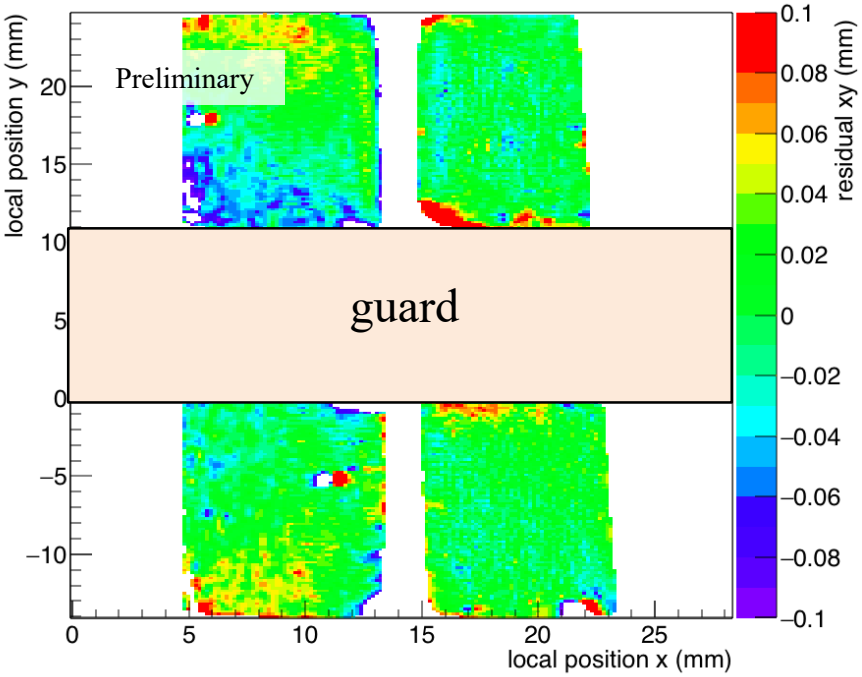

Figure 11. Averaged residuals in the xy plane over the quad detector surface.

5. Conclusions

Starting with the GridPix detector using a single Timepix3 chip, we have developed and tested the quad, a detector based on four chips. The detector has an active surface of 68.9% and can be used as a building block to cover large detection areas. Since the analysis of a recent testbam experiment is still ongoing, only preliminary performance results were presented. First results for the single electron resolution in the transverse and longitudinal plane are similar to the results obtained for the single chip.

While the single hit based results shown in this report do not look exceptional at a first glance, the advantages of the GridPix technology become more clear if one considers large TPC detectors. In that case a 1 meter track will have of the order of 10k hits. In the presence of a magnetic field of e.g. 3.5 T the transverse diffusion is an order of magnitude smaller. Therefore, a pixel TPC using the GridPix technology can provide very accurate tracking.

Also for the detection of microscopically small phenomena like delta rays, photon conversions, and rare events the GridPix technology is very well suited since it delivers with the smallest density of detection medium the highest possible resolution.

As a demonstration of the capabilities of the GridPix technology, a module with 2 x 4 quads is in preparation to serve as a large high-resolution TPC plane with a 62 cm^2 active area.

References

[1] P. Colas et al., The readout of a GEM- or micromegas equipped TPC by means of the Medipix2 CMOS sensor as direct anode, Nucl. Instrum. Meth. A535 (2004) 506.
M. Campbell, et al., The Detection of single electrons by means of a micromegas-covered MediPix2 pixel CMOS readout circuit, Nucl. Instrum. Meth. A540 (2005) 295.
J. Kaminski et al., GridPix detectors - introduction and applications. Nucl. Instrum. Meth. A845 (2017) 233.
[2] T. Poikela et al., Timepix3: a 65K channel hybrid pixel readout chip with simultaneous ToA/ToT and sparse readout, Journal of Instrumentation, Vol. 9 (2014) C05013.

[3] I. Rubinskiy on behalf of EUDET and AIDA consortia, An EUDET/AIDA pixel beam telescope for detector development, Physics Procedia, Vol. 37 (2012) 923.
H. Jansen et al., Performance of the EUDET-type beam telescopes. EPJ Techniques and Instrumentation, (2016) 3:7.
[4] C. Ligtenberg et al. Performance of a GridPix detector based on the Timepix3 chip. Nucl. Instrum. Meth. A908 (2018) 18.
[5] J. Visser et al., SPIDR: a read-out system for Medipix3 & Timepix3. Journal of Instrumentation, 10(12) (2015) C12028.